2022 IEEE Conference on Control Technology and Applications (CCTA)
August 22-25, 2022. Trieste, Italy

A Sliding Mode Observer-based Limit Cycle Oscillation Suppression using a Robust Active Flow Control Technique

Krishna Bhavithavya Kidambi[1], Madhur Tiwari[2], Anu Kossery Jayaprakash[3], William MacKunis[3] and Vladimir Golubev[4]

***Abstract*— This paper presents a sliding mode observer (SMO)-based robust control method, which achieves simultaneous estimation, fluid flow velocity regulation and limit cycle oscillation (LCO) suppression in a flexible airfoil. The proposed control design is based on a dynamic model that incorporates the fluid structure interactions (FSI) in the airfoil. The FSI describe how the flow field velocity at the surface of a flexible structure gives rise to fluid forces acting on the structure. In the proposed control method, the LCO are controlled via control of the flow field velocity near the surface of the airfoil using surface-embedded synthetic jet actuators. The flow field velocity is expressed using a proper orthogonal decomposition based reduced-order flow model that formally incorporates the actuation effects of synthetic jet actuator. Specifically, this flow field velocity profile is driven to a desired time-varying profile, which results in a LCO-stabilizing fluid forcing function acting on the airfoil. A sliding mode observer is designed to estimate the unmeasurable states in the reduced-order model of the actuated flow field dynamics. The SMO is rigorously proven to achieve local finite-time estimation of the unmeasurable state in the presence of the parametric uncertainty in the SJA. A Lyapunov-based stability analysis is used to prove that the active flow control system asymptotically converges to the LCO-stabilizing forcing function that suppresses the LCO. Numerical simulation results demonstrate that the augmented observer provides a reduction in the control effort required to stabilize the LCO.**

2022 IEEE Conference on Control Technology and Applications (CCTA) | 978-1-6654-7338-5/22/$31.00 ©2022 IEEE | DOI: 10.1109/CCTA49430.2022.9966001

I. Introduction

The interaction between a flexible structure and the fluid surrounding it is referred to as fluid structure interactions (FSI). A detailed understanding of FSI is of critical importance in numerous applications in aeronautical and aerospace systems, renewable energy systems, and marine offshore engineering [1], [2], [3]. A particularly important application of FSI is in the development of limit cycle oscillation (LCO) suppression control systems for unmanned aircraft. Indeed, a thorough understanding of the FSI and LCO can lead to significant improvements in the aerodynamic characteristics of aircraft, such as lift enhancement and drag reduction. While standard LCO suppression control in aircraft wings is achieved using deflection surfaces (e.g., ailerons, rudders), the contribution of this paper is the analysis of a sliding mode observer and robust control system that achieves LCO suppression via control of the wing boundary-layer flow field velocity.

LCO (or flutter) are self-excited aeroelastic instabilities that can have a detrimental effect on aircraft flight performance and can even lead to catastrophic failures [4], [5]. A thorough review of research and development in LCO suppression technology over 50 years is presented in [4]. To achieve the boundary-layer flow control, synthetic jet actuators (SJA) have become a popular choice due to their small size, cost-effectiveness, and easy implementation [5].

SJA have been widely used in recent flow control and LCO suppression research [6], [7], [8]. The reader is referred to [6] for a detailed analysis into origins, applications and current state of the art about SJA. In [7], a span-wise array of SJAs are used for control of boundary layer separation and the influence of geometrical, operational parameters on the flow separation control are investigated. An active flow control method to achieve pitch-roll-yaw attitude control at a high angle of attack when the stall occurs is proposed in [8] using SJA. One of the primary challenge in SJA-based control design is that the input-output characteristic of the SJA contain parametric uncertainty and are nonlinear. Specifically, the relationship between the virtual deflection angle and the SJA input voltage is an uncertain nonlinear function. Additional challenges arise due to the nature of the mathematical models of the flow dynamics.

Active flow control techniques have gained a lot of attention recently [9], [10], [11], due to their significant advantages by virtue of their capability to react in real time to time-varying sensor measurements of flow field properties. A detailed review of active flow control for UAVs can be found in [9]. To facilitate active flow control design, proper orthogonal decomposition (POD)-based model order reduction technique can be used to express the Navier-Stokes PDEs as a finite set of ordinary differential equations (ODEs) [10]. It has been shown that this model order reduction technique is capable of approximating the flow field dynamics using only a few states (i.e., POD modes) [11], and this reduced-order model is in a form that is amenable to control design. Furthermore, the Galerkin coefficients are not directly measurable. To overcome this problem, a sliding mode observer (or estimator) can be designed to estimate the unknown coefficients using flow field velocity measurements.

Sliding mode observer-based estimation methods have

[1]Krishna Bhavithavya Kidambi is an Assistant Professor in the Department of Mechanical and Aerospace Engineering, University of Dayton, Dayton, OH 45469. kkidambi1@udayton.edu

[2]Madhur Tiwari is an Assistant Professor in the Department of Aerospace, Physics And Space Sciences, Florida Institute of Technology, Melbourne, FL 32901. mtiwari1@fit.edu

[3]Anu Kossery Jayaprakash, William MacKunis are with Physical Sciences Department, Embry-Riddle Aeronautical University, Daytona Beach, FL 32114. kosserya@my.erau.edu, mackuniw@erau.edu

[4]Vladimir Golubev is a Professor in the Department of Aerospace Engineering, Embry-Riddle Aeronautical University, Daytona Beach, FL 32114. vladimir.golubev@erau.edu

been utilized extensively due to the advantage of fast convergence and inherent robustness to model uncertainty [12], [13]. In this paper, a finite-time SMO is proposed for dynamic systems containing both a nonstandard measurement equation and input-multiplicative parametric uncertainty.

The main contributions of the paper are summarized as

1) Development of a sliding mode observer that achieves finite time state estimation of the reduced-order flow dynamic model under SJA parametric uncertainty.
2) Development of robust control algorithm, which formally incorporates FSI with a POD-based reduced-order flow dynamic model to achieve LCO suppression in a flexible aircraft wing
3) The proposed theoretical contributions are validated through numerical simulations (which incorporate detailed models of the LCO and reduced-order flow dynamics combined with an SMO) to demonstrate proof of concept numerically.

II. Mathematical Model

In this section, the mathematical model of LCO dynamics in an airfoil and the flow field dynamics based on Navier-Stokes equations are presented. Section II-A describes the LCO dynamics of a foil in the presence of fluid forces. In II-B, a detailed description of the actuated fluid flow model using incompressible Navier-Stokes is presented and a POD-based model reduction technique is utilized to recast the incompressible Navier-Stokes equations as finite set of nonlinear ODEs. Fig. 1 shows the block diagram of the proposed closed-loop system.

A. LCO Dynamic Model

The equation of motion describing the LCO dynamics, in the presence of a fluid forcing function are expressed as [14]

$$M(s)\ddot{p}(s,t) + C(\dot{p}(s,t)) + K(p(s,t)) = BF_{fluid}(s,t) \quad (1)$$

where $p(t) \triangleq \begin{bmatrix} h(t) & \alpha(t) \end{bmatrix}^T \in \mathbb{R}^2$ denotes the LCO displacement vector containing plunging ($h(t)$) and pitching ($\alpha(t)$) displacements, $s \in \mathbb{R}$ is the linear position along the structure (i.e., wing), $M(s) \in \mathbb{R}^{2\times 2}$ is the inertia matrix of the wing, and $C(*) \in \mathbb{R}^2$ and $K(*) \in \mathbb{R}^2$ denote viscous damping and stiffness functions, respectively. In (1), $F_{fluid}(s,t) \in \mathbb{R}$ denotes the fluid forces acting on the wing, and $B \in \mathbb{R}^2$ is a constant input gain vector.

In the LCO dynamic model given by (1), the fluid forcing function $F_{fluid}(s,t)$ can be mathematically expressed as the product of the boundary-layer turbulence velocity $a(s,t)$ and a position-dependent function $b(s)$ as [14]

$$F_{fluid}(s,t) = \rho d c_d U(s) a(s,t). \quad (2)$$

In (2) the fluid forcing function is directly dependent on the flow turbulence $a(s,t)$ near the surface of the wing. The variables ρ denotes the density of the air/fluid, d is the wing cross-sectional area, c_d is the drag coefficient and $U(s)$ denotes the mean air flow velocity near the surface of the wing.

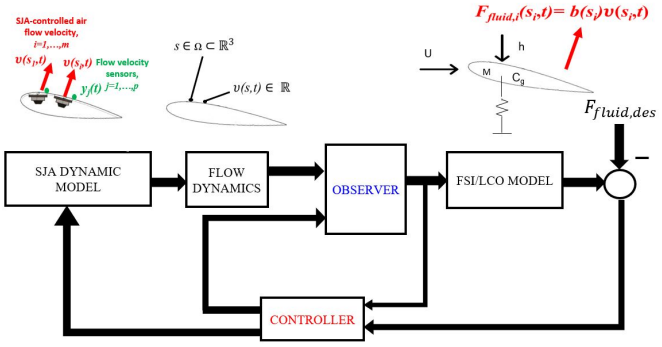

Fig. 1. A block diagram illustrating the proposed nonlinear control method for simultaneous flow control and LCO suppression

B. Flow Dynamics Reduced-order Model

In this section, a POD-based model reduction technique is utilized to recast the incompressible Navier-Stokes equations as a finite set of nonlinear ODEs. By expressing the Navier-Stokes PDEs as a set of ODEs, an approximate dynamic model for the flow dynamics will be obtained, which is more amenable to control design.

The incompressible Navier-Stokes equations are given as [15]

$$\nabla \cdot a = 0, \qquad \frac{\partial a}{\partial t} = -(a \cdot \nabla)a + \nu\nabla^2(a) - \nabla p, \quad (3)$$

where $a(s,t) : \Omega \times [0,\infty) \to \mathbb{R}$ denotes the velocity of the flow field over a spatial domain $s \in \Omega$; $p(s,t) \in \mathbb{R}$ is the space and time-dependent pressure of the flow field over Ω; ∇ denotes the spatial gradient; and $\nu \triangleq \frac{1}{Re}$ is the kinematic viscosity, where Re denotes the Reynolds number.

Proper orthogonal decomposition (POD), is used to obtain lower-dimensional dynamic models for fluid flow. In the POD-based model order reduction method, the flow velocity field $a(s,t)$ is expanded as a weighted sum of actuated and unactuated POD modes defined in the spatial domain Ω as [16], [17]

$$a(s,t) = a_0(s,t) + \sum_{i=1}^{n} x_i(t)\varphi_i(s) + \sum_{i=1}^{m} \chi_i(t)\phi_i(s) \quad (4)$$

In (4), $\varphi_i(s) \in \mathbb{R}$ denote the POD modes; $x_i(t)$, $i = 1, ..., n$, are time-varying coefficients resulting from the modal decomposition; and $a_0(s,t) \in \mathbb{R}$ denotes the mean flow velocity over Ω, where $\phi_i(s) \in \mathbb{R}$ denote the actuation modes, and $\chi_i(t) \in \mathbb{R}$ denote actuation values (i.e., control inputs).

For the control design presented here, it will be assumed that an input separation method in [17] is utilized to expand the flow field in terms of baseline (unactuated) POD modes and actuation modes. The baseline POD modes are extracted using a standard POD procedure as described in Section II-B, whereas the actuation modes are built using an optimization algorithm similar to that in [17]. By substituting the actuated modal decomposition in (4) into (3), the actuated

reduced-order flow dynamics can be expressed in terms of an auxiliary ("virtual") control input $u(t)$ as

$$\dot{x} = f(x) + g(x)u, \qquad y = h(x) \tag{5}$$

The reader is referred to [18], for a detailed mathematical derivation of the reduced-order actuated flow model and is omitted her for brevity.

III. SJA-based Control Model Derivation

In this section, a reduced order POD-based flow field dynamic model will be augmented to include the effects of SJA actuation. The uncertain control model is a key feature of the proposed observer and flow control design, which enables us to derive a nonlinear control law that is proven to compensate for the parametric uncertainty in the SJA actuators.

A. SJA Actuator Model

The relation between the virtual control surface deflection angle produced by an i^{th} SJA array (i.e., $u(t)$ in (5)) and the corresponding SJA array input voltages can be expressed using the empirically determined model as [19]

$$u_i(t) = \theta^{\star}_{2i} - \frac{\theta^{\star}_{1i}}{v_i(t)}, \qquad i = 1, 2, ..., m. \tag{6}$$

where $u_i(t) \in \mathbb{R}$ denotes the virtual surface deflection due to i^{th} SJA array. In (6), $v_i(t) \triangleq A^2_{ppi}(t) \in \mathbb{R}$, where A_{ppi} represents the peak-to-peak voltage magnitude applied to the i^{th} SJA array; and $\theta^{\star}_{1i}$, $\theta^{\star}_{2i} \in \mathbb{R}$ are uncertain physical parameters in [V-deg] and [deg] respectively. To address the parametric uncertainty inherent in the SJA model, the voltage input signal $v_i(t)$ can be designed using the robust-inverse control structure [19]

$$v_i(t) = \frac{\hat{\theta}_{1i}}{\hat{\theta}_{2i} - u_{di}(t)} \tag{7}$$

where, $u_{di}(t) \in \mathbb{R}$, for $i = 1, ..., m$, are auxiliary control signals and $\hat{\theta}_{1i}$, $\hat{\theta}_{2i} \in \mathbb{R}^+$ are constant, feedforward *best-guess* estimates of the uncertain parameters $\theta^{\star}_{1i}$ and $\theta^{\star}_{2i}$.

Remark 1: **(Singularity Avoidance)** Based on the robust-inverse control structure in (7), the SJA voltage input signal $v_i(t)$ will encounter singularities when $u_{di}(t) = \hat{\theta}_{2i}$. To avoid these singularities, the auxiliary control signals $u_{di}(t)$, for $i = 1, ..., m$, can be designed using a singularity avoidance algorithm [20].

After substituting (6) and (7) into (5), the SJA-based control model can be expressed as

$$\dot{x} = f(x) + \Xi_B + \Omega u_d(t) \tag{8}$$

where $u_d(t) \triangleq [u_{d1}(t), ..., u_{dm}(t)]^T \in \mathbb{R}^m$, and expressions for the uncertain constant auxiliary terms $\Xi_B \in \mathbb{R}^n$ and $\Omega \in \mathbb{R}^{n \times m}$ are summarized in the following remark.

To address the problem of uncertainty in the input-multiplicative matrix Ω in (8), the auxiliary control signal $u_d(t)$ is designed as

$$u_d(t) = \hat{\Omega}^{\#} \mu(t) \tag{9}$$

where $\hat{\Omega} \in \mathbb{R}^{n \times m}$ denotes a feedforward estimate of Ω, and $[\cdot]^{\#}$ denotes the pseudoinverse of a (nonsquare) matrix. After substituting (9) into (8), the open loop SJA-based system can be expressed as

$$\dot{x} = f(x) + \Xi_B + \tilde{\Omega}\mu(t) \tag{10}$$

where $\tilde{\Omega} \triangleq \Omega\hat{\Omega}^{\#} \in \mathbb{R}^{n \times n}$. Heuristically, the uncertain matrix $\tilde{\Omega}$ represents the deviation between the actual SJA parameters $\theta^{\star}_{1i}$ and their constant estimates $\hat{\theta}_{1i}$, for $i = 1, ..., m$.

Property 1: The uncertain matrix $\tilde{\Omega}$ can be decomposed as

$$\tilde{\Omega} = \Gamma + \Delta(t) \tag{11}$$

where $\Gamma \in \mathbb{R}^{n \times n}$ denotes an $n \times n$ identity matrix and $\Delta(t) \in \mathbb{R}^{n \times n}$ denotes off-diagonal uncertain "mismatch" matrix.

Assumption 1: Approximate model knowledge of the uncertain parameters is available such that the parameter mismatch matrix $\tilde{\Omega}$ is diagonally dominant in the sense that

$$\inf_t\{\lambda_{min}(\Gamma)\} - \sup_t\{\|\Delta(t)\|_{i\infty}\} > \varepsilon \tag{12}$$

where $\varepsilon \in \mathbb{R}^+$ is a known bounding constant, and $\|\cdot\|_{i\infty}$ denotes the induced infinity norm of a matrix.

Assumption 2: The initial conditions of the state and estimate satisfy $|x(0) - \hat{x}(0)| \leq \epsilon_0$, where $|(\cdot)|$ denotes a standard 1-norm of a vector and ϵ_0 is a known bounding constant.

By substituting (11) into (10), the SJA-based flow dynamic model can be expressed as

$$\dot{x} = f(x) + \Xi_B + \mu(t) + \Delta(t)\mu(t), \qquad y = h(x), \tag{13}$$

Remark 2: The control objective in this paper is based on driving the fluid forcing function to a desired fluid forcing function, which is designed in a separate step based on the objective of regulating LCO. The fluid forcing function in (2) can be approximated using POD as

$$F_{fluid} = b(s)a(s,t) \simeq b(s)y(t) = b(s)h(x), \tag{14}$$

where $y(t)$ is the output of the flow dynamic model described in (13). The approximation accuracy can be made arbitrarily accurate by adjusting the number of POD modes which are defined in (4).

IV. Observer Design

In this section, a SMO design is presented, which achieves finite-time state estimation for the uncertain system described in (13) using only the available sensor measurements (i.e., $y(t)$).

To facilitate the following SMO design and convergence analysis, a vector of output signals is defined as

$$\begin{aligned} H(x,\mu) &\triangleq \begin{bmatrix} h_1(x) & h_2(x,\mu) & \cdots & h_n(x,\mu) \end{bmatrix}^T \\ &= \begin{bmatrix} h(x) & L_f h(x) & \cdots & L_f^{n-1} h(x) \end{bmatrix}^T \end{aligned} \tag{15}$$

where $L^i_f h(x)$ denotes the i^{th} Lie derivative of the output function $h(x)$ [21], along the direction of the vector field $f(x,\mu)$. Note that $h_1(x) = h(x)$ does not include the

measurable input signal $\mu(t)$ based on the output equation in (13).

Condition 1 (Observability): The closed loop dynamics in (13) must satisfy the observability condition

$$\text{rank}\left(\mathcal{O}(x,\mu)\right) = n, \ \forall \ x \in \mathbb{R}^n, \tag{16}$$

where the observability matrix $\mathcal{O}(x,\mu) \triangleq \frac{\partial H(x,\mu)}{\partial x} \in \mathbb{R}^{n\times n}$ and $\left|\det\left(\frac{\partial H(x)}{\partial x}\right)\right| \geq \epsilon > 0$. The observability condition given in (16) can be ensured through judicious sensor placement. A detailed analysis on sensor placement and the number of sensors required (varies according to the application) for flow control has been described in [22].

Provided Condition 1 and Assumptions 1 and 2 are satisfied, the sliding mode observer that estimates the full state $x(t)$ for the uncertain flow dynamic system in (13) can be designed as

$$\dot{\hat{x}} = f(\hat{x}) + \mathcal{O}^{-1}(\hat{x},\mu)\,\mathcal{K}(\hat{x},\mu)\{sgn(V(t) - H(\hat{x}))\} + \mu(t) \tag{17}$$

where $H(\cdot)$ is defined in (15), and $\mathcal{O}(\hat{x},\mu)$ is introduced in (16). In (17), the elements of the auxiliary vector $V(t) = [v_1(t), ..., v_n(t)]^T \in \mathbb{R}^n$ are defined via the recursive form

$$v_1(t) = h_1(x) \tag{18}$$

$$v_{i+1}(t) = \kappa_i\left\{sgn[v_i(t) - h_i(\hat{x})]\right\}_{eq} + \frac{\partial h_i(\hat{x})}{\partial x}\mu(t) \tag{19}$$

for $i = 1, ..., n-1$ and $\{\text{sgn}[\cdot]\}_{eq}$ denotes a continuous equivalent value operator of the discontinuous signum function [18]. The observer in (17) will be proven to achieve finite-time state estimation in the presence of the input-multiplicative SJA parametric uncertainty through the design of the sliding gain matrix $\mathcal{K}(\hat{x},\mu) \in \mathbb{R}^{n\times n}$, which has the general form

$$\mathcal{K}(\hat{x},\mu) = \text{diag}[\kappa_1(\hat{x},\mu), ..., \kappa_n(\hat{x},\mu)] \tag{20}$$

where $\kappa_i(\hat{x},\mu) \in \mathbb{R}$, for $i = 1, ..., n$, denote sliding mode observer gains which are designed as

$$\kappa_i(\hat{x},\mu) = \beta_{1,i} + \beta_{2,i}\|\mu\|. \tag{21}$$

Theorem 1: **(Observer Convergence)** The observer given in (17) achieves local finite-time estimation of the state $x(t)$ in the sense that $\hat{x}(t) \equiv x(t)$ for $t \geq t_n$, where $t_n < \infty$ is a calculable time instant.

Proof: Proof of Theorem 1 can be found in [18] and is omitted here for brevity. ■

V. Control Development

The control objective is to design the control signal $\mu(t)$ to regulate the fluid forcing function F_{fluid} defined in (14) to a desired fluid forcing function $F_{fluid,des}$, which is defined as

$$F_{fluid,des} = b(s)y_d(t) \tag{22}$$

where $y_d(t)$ is the desired flow field velocity output that suppresses LCO. To quantify the control objective, a tracking error $e(t) \in \mathbb{R}$ and an auxiliary tracking error $r(t) \in \mathbb{R}$ are defined as

$$e(t) = F_{fluid} - F_{fluid,des}, \qquad r(t) = \dot{e} + \alpha e, \tag{23}$$

where $\alpha \in \mathbb{R}$ is a positive, constant control gain. Thus, the control objective can be stated mathematically as $e(t) \to 0$

A. Open Loop Error System

Taking the time derivative of $r(t)$ and using the definition of (23), the open loop error dynamics can be expressed as

$$\dot{r} = \tilde{N}(t) + N_d(t) + \tilde{\Omega}_1\dot{\mu}(t) + b(s)\dot{\Delta}(t)\mu(t) - e, \tag{24}$$

where $\tilde{\Omega}_1 \equiv b(s)\tilde{\Omega}$ and the unknown, unmeasurable auxiliary functions, $\tilde{N}(t)$, $N_d(t) \in \mathbb{R}$ are defined as

$$\tilde{N} = b(s)\tfrac{\partial f(x)}{\partial x}\dot{x} + \alpha(r - \alpha e) + e, \tag{25}$$

$$N_d = -\ddot{F}_{fluid,des} \tag{26}$$

The motivation for the separation of terms in (V-B), (25) and (26) is based on the fact that the following inequalities can be developed

$$\|\tilde{N}\| \leq \rho(\|z\|)\|z\|, \qquad \|N_d\| \leq \zeta_{N_d}, \qquad \|\dot{N}_d\| \leq \zeta_{\dot{N}_d}, \tag{27}$$

where ρ, ζ_{N_d}, $\zeta_{\dot{N}_d} \in \mathbb{R}^+$ are known bounding constants; and $z(t) \in \mathbb{R}^2$ is defined as

$$z(t) \triangleq \begin{bmatrix} e(t) & r(t) \end{bmatrix}. \tag{28}$$

Note that the upper bound on $\|\tilde{N}(t)\|$ in (27) can be derived from (25), along with the definitions in (14), (22), and (23).

B. Closed-Loop Error System

Based on the open-loop error system dynamics in (), the control $\mu(t)$ is defined via

$$\dot{\mu}(t) = -k_u\|\mu(t)\|sgn(r) - (k_s+1)r - k_\gamma sgn(r) \tag{29}$$

where $k_u, k_s, k_\gamma \in \mathbb{R}$ are positive, constant control gains. After substituting (29) into (), the closed-loop error dynamics is rewritten as

$$\dot{r} = \tilde{N} + N_d - \tilde{\Omega}_1 k_u\|\mu(t)\|sgn(r) - \tilde{\Omega}_1(k_s+1)r - \tilde{\Omega}_1 k_\gamma sgn(r) + b(s)\dot{\Delta}(t)\mu(t) - e. \tag{30}$$

VI. Stability Analysis

Theorem 2: The robust nonlinear control law given in (7), (9), and (29) ensures that all system signals remain bounded throughout closed-loop operation, and that the fluid forcing function tracking error is asymptotically regulated in the sense that

$$\|e(t)\| \to 0 \qquad \text{as} \qquad t \to \infty, \tag{31}$$

provided the control gain k_u, k_s and k_γ introduced in (29) are selected according to the conditions

$$k_s > \frac{\rho^2\|z\|}{4\varepsilon min(\alpha,\varepsilon)}, \qquad k_u \geqslant \frac{\varepsilon_1}{\varepsilon}, \qquad k_\gamma \geqslant \frac{\zeta_{N_d}}{\varepsilon}. \tag{32}$$

Proof: Let $V(z,t) : \mathbb{R}^2 \to \mathbb{R}$ be a non-negative function defined as

$$V = \frac{1}{2}e^T e + \frac{1}{2}r^T r \tag{33}$$

After taking the time derivative of (33) and using (11), (23), (30) and using Assumptions 1 and Property 1, and the bounding inequalities in (27) and the gain conditions in (32), the bracketed terms are positive and by completing the squares and the upper bound can be expressed as $\dot{V}(z,t)$ can be upper bounded as

$$\dot{V}(z,t) \leq -\left[min(\alpha,\epsilon) - \frac{\rho^2(\|z\|)}{4\varepsilon(k_s)}\right]\|z^2\| \tag{34}$$

Provided the gain condition in (32) is satisfied, (33) and (34) can be used to show that $V(t) \in \mathcal{L}_\infty$; hence, $e(t)$, $r(t) \in \mathcal{L}_\infty$. Given that $e(t)$, $r(t) \in \mathcal{L}_\infty$, a standard linear analysis technique can be used along with (23) to show that $\dot{e}(t) \in \mathcal{L}_\infty$. Since $e(t)$, $\dot{e}(t) \in \mathcal{L}_\infty$, (23) can be used along with the assumption that $y_d(t)$, $\dot{y}_d(t) \in \mathcal{L}_\infty$ to prove that $x(t)$, $\dot{x}(t) \in \mathcal{L}_\infty$. Given that $x(t)$, $\dot{x}(t) \in \mathcal{L}_\infty$, (5) can be used along with the Assumption 1 to prove that the control input $\mu(t) \in \mathcal{L}_\infty$. Since $r(t) \in \mathcal{L}_\infty$, Assumption 1 can be used along with (29) to prove that $\dot{\mu}(t) \in \mathcal{L}_\infty$.

The definition of $V(z,t)$ in (33) can be used along with the inequality (34) to show that $V(z,t)$ can be upper-bounded as

$$\dot{V}(z,t) \leq -cV(z,t) \tag{35}$$

provided the sufficient condition in (32) is satisfied. Hence, (28),(33) and (35) can be used to conclude that

$$\|e(t)\| \leq \|z(0)\|e^{-\frac{c}{2}t} \qquad \forall \;\; t \in [0,\infty). \tag{36}$$

VII. Simulation Results

A numerical simulation was performed to demonstrate the performance of the proposed control law in (29) using the observer design in (17). The simulation tests the capability of the proposed controller using the estimated states to regulate fluid forcing function in (2) to desired fluid forcing function that suppresses the plunging LCO and at the same time compensate for the input-multiplicative parametric uncertainty resulting from SJ actuators.

A. Flow and LCO Dynamic Model

The reduced-order model flow dynamic equations and the corresponding POD parameters can be found in [18]. The LCO dynamic model equation (cf. Equation (1)) and the corresponding parameters used in the simulation can be [5] and are omitted for brevity.

TABLE I

Initial Conditions for States and Estimates, Observer Gains

States ($x(t)$)	7.5	6	3	2
Estimates ($\hat{x}(t)$)	8	4	2	1.5
Gains	β_{11} = 5	β_{12} = 3	β_{13} = 3	β_{14} = 3
Gains	β_{21} = 0.1	β_{22} = 0.1	β_{23} = 0.1	β_{24} = 0.1

The initial conditions of the states, estimates and the observer gains $\kappa_{1,i}$ and $\kappa_{2,i}$ for $i = 1,2,3,4$ are provided in Table I. The control gain values were selected as $k_s = 10$, $k_u = 0.3$, $\alpha = 0.25$, and $k_\gamma = 0.5$. A Monte Carlo-type simulation was created, which shows the results of the closed-loop AFC system under three different sets of values for the uncertain SJA parameters $\theta^\star_{1i}, \theta^\star_{2i}$. Table II shows the deviation of each SJA parameters from its nominal value (up to 20%).

TABLE II

SJA parameters and their estimates for all three cases

Nominal Values	$\hat{\theta}_{1i}$	32.7, 29.7	$\hat{\theta}_{2i}$	16.4, 15.8
Case 1	$\theta^\star_{1i}$	32.3, 31.8	$\theta^\star_{2i}$	16.5, 16.5
Case 2	$\theta^\star_{1i}$	32.0, 26.7	$\theta^\star_{2i}$	16.2, 14.2
Case 3	$\theta^\star_{1i}$	31.7, 23.7	$\theta^\star_{2i}$	16.0, 12.6

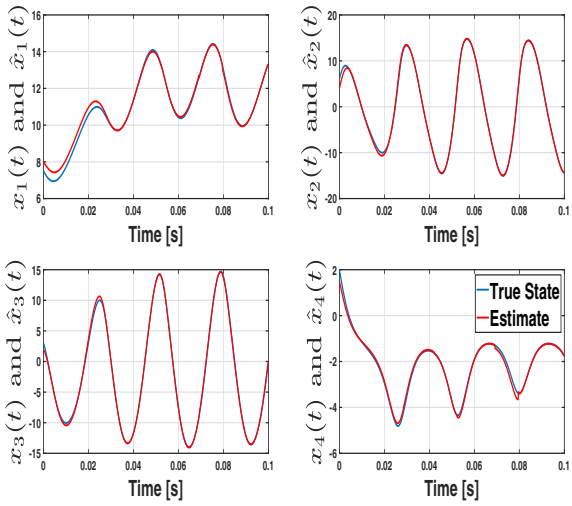

Fig. 2. Zoomed-in Plots showing initial convergence phase of the states(blue) and estimates(red) using the observer in (17).

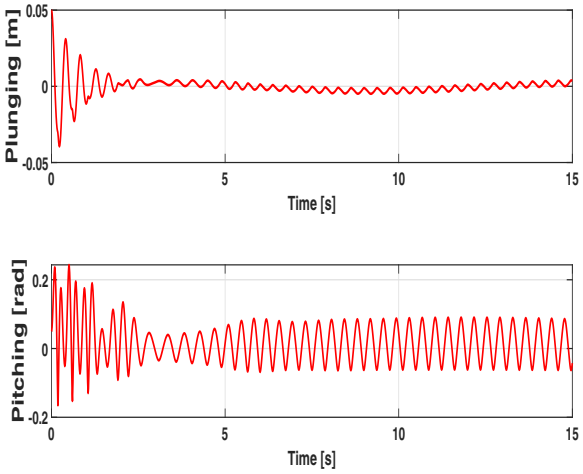

Fig. 3. Open-loop plunging and pitching response of the LCO system.

The simulation results are summarized in Fig. 2-4. Fig.

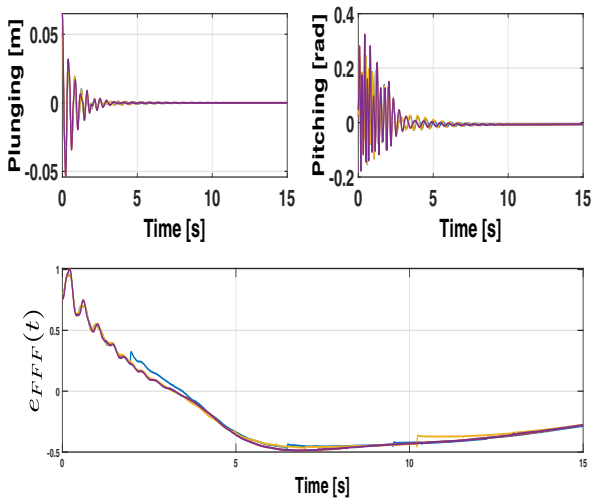

Fig. 4. Monte Carlo-type simulation results for 4 different initial conditions and uncertain SJA parameters. [Plunging (top-left), pitching (top-right) and error (bottom) in fluid forcing function]

2 shows the zoomed-in initial transient response of the SMO. The open-loop plunging and pitching responses of the LCO are shown in Fig. 3. Fig. 4 shows the Monte Carlo closed-loop pitching (top-left), plunging (top-right) and error (bottom) in fluid forcing function for four different initial conditions and uncertain SJA parameters. The results clearly demonstrate the capability of proposed observer to compensate for SJA uncertainty with a reduced control effort to asymptotically regulate LCO via the control of the boundary-layer flow velocity.

VIII. Conclusion

A sliding mode observer-based robust active flow control method is developed, which is rigorously proven to asymptotically suppress LCO in a flexible wing section by using SJA to drive the wing boundary-layer flow velocity to a desired LCO-suppressing flow velocity profile. To achieve the result, a sliding mode observer is designed to estimate the flow field velocity in finite time and a LCO dynamic model is utilized along with detailed mathematical models for the FSI, SJA, and the POD-based reduced-order flow dynamics. A Lyapunov-based stability analysis is utilized to prove asymptotic convergence and tracking of a desired LCO-suppressing fluid forcing function. Numerical simulation demonstrate the observer and the control formulation shows a reduction in the control effort to achieve asymptotic regulation of LCO via boundary-layer flow control.

References

[1] R. K. Jaiman and V. Joshi, *Computational Mechanics of Fluid-Structure Interaction*. Springer, 2022.

[2] S. Kaneko and S. Yoshimura, "Fluid–structure–control interaction simulation of flutter control problems," *Finite Elements in Analysis and Design*, vol. 203, p. 103722, 2022.

[3] A. Eldemerdash and T. Leweke, "Fluid–structure interaction of a flexible rotor in water," *Journal of Fluids and Structures*, vol. 103, p. 103259, 2021.

[4] E. Livne, "Aircraft active flutter suppression: State of the art and technology maturation needs," *Journal of Aircraft*, vol. 55, no. 1, pp. 410–452, 2017.

[5] N. Ramos-Pedroza, W. MacKunis, and V. Golubev, "A robust nonlinear output feedback control method for limit cycle oscillation suppression using synthetic jet actuators," *Aerospace Science and Technology*, vol. 64, pp. 16–23, 2017.

[6] P. Walimbe, A. Agrawal, and M. B. Chaudhari, "Flow characteristics and novel applications of synthetic jets-a review," *Journal of Heat Transfer*, 2021.

[7] M. Ja'fari, A. J. Jaworski, and A. Rona, "Application of synthetic jet arrays for flow separation control on a circular "hump" model," *Experimental Thermal and Fluid Science*, vol. 131, p. 110543, 2022.

[8] C. Li, T. Zhang, and J. Yang, "Attitude control of aircraft using only synthetic jet actuators when stall occurs," *IEEE Access*, vol. 6, pp. 37910–37917, 2018.

[9] D. Greenblatt and D. R. Williams, "Flow control for unmanned air vehicles," *Annual Review of Fluid Mechanics*, vol. 54, pp. 383–412, 2022.

[10] K. Taira, M. S. Hemati, S. L. Brunton, Y. Sun, K. Duraisamy, S. Bagheri, S. T. Dawson, and C.-A. Yeh, "Modal analysis of fluid flows: Applications and outlook," *AIAA journal*, vol. 58, no. 3, pp. 998–1022, 2020.

[11] K. Taira, S. L. Brunton, S. T. Dawson, C. W. Rowley, T. Colonius, B. J. McKeon, O. T. Schmidt, S. Gordeyev, V. Theofilis, and L. S. Ukeiley, "Modal analysis of fluid flows: An overview," *Aiaa Journal*, pp. 4013–4041, 2017.

[12] R. Franco, H. Ríos, D. Efimov, and W. Perruquetti, "Adaptive estimation for uncertain nonlinear systems with measurement noise: A sliding-mode observer approach," *International Journal of Robust and Nonlinear Control*, vol. 31, no. 9, pp. 3809–3826, 2021.

[13] H. Ríos, R. Franco, A. F. de Loza, and D. Efimov, "A high-order sliding-mode adaptive observer for uncertain nonlinear systems," *IEEE Transactions on Automatic Control*, 2021.

[14] A. Torrielli, F. Tubino, and G. Solari, "Effective wind actions on ideal and real structures," *Journal of Wind Engineering and Industrial Aerodynamics*, vol. 98, no. 8-9, pp. 417–428, 2010.

[15] G. Batchelor, *An introduction to fluid dynamics*. Cambridge university press, 2000.

[16] I. Akhtar, A. H. Nayfeh, and C. J. Ribbens, "On the stability and extension of reduced-order galerkin models in incompressible flows," *Theoretical and Computational Fluid Dynamics*, vol. 23, no. 3, pp. 213–237, 2009.

[17] C. Kasnakoğlu, R. C. Camphouse, and A. Serrani, "Reduced-order model-based feedback control of flow over an obstacle using center manifold methods," *Journal of Dynamic Systems, Measurement, and Control*, vol. 131, no. 1, p. 011011, 2009.

[18] K. Bhavithavya Kidambi, W. MacKunis, S. V. Drakunov, and V. Golubev, "Sliding mode estimation and closed-loop active flow control under actuator uncertainty," *International Journal of Robust and Nonlinear Control*, vol. 30, no. 16, pp. 6645–6660, 2020.

[19] D. Deb, J. Burkholder, and G. Tao, "Synthetic jet actuators and arrays: Modeling and control," in *Adaptive Compensation of Nonlinear Actuators for Flight Control Applications*, pp. 11–41, Springer, 2022.

[20] S. T. Mondschein, G. Tao, and J. O. Burkholder, "Adaptive actuator nonlinearity compensation and disturbance rejection with an aircraft application," in *American Control Conference (ACC), 2011*, pp. 2951–2956, IEEE, 2011.

[21] A. Isidori, *Nonlinear control systems*. Springer Science & Business Media, 2013.

[22] B. Jin, S. J. Illingworth, and R. D. Sandberg, "Optimal sensor and actuator placement for feedback control of vortex shedding," *Journal of Fluid Mechanics*, vol. 932, 2022.